FIRST MINERAL CHEMISTRY DATA ON THE EXOTIC IGNEOUS CLASTS FROM THE CRETACEOUS SUCCESSIONS OF THE MOLDAVIDES (EASTERN CARPATHIANS, ROMANIA): INSIGHTS INTO MAGMA EVOLUTION AND GEOTECTONIC SETTING

Sarolta LŐRINCZ[1,2], Marian MUNTEANU[1,2], George DINCĂ[1]

[1]*Geological Institute of Romania, 1 Caransebeș St., 012271, Bucharest, Romania*
[2]*Institute of Geodynamics Sabba S. Ștefănescu of the Romanian Academy, 19-21 Jean-Louis Calderon St., 020032, Bucharest, Romania*

DOI: 10.xxxx

Abstract. Igneous (granites, granodiorites and rhyolites) clasts of exotic (i.e. non-Carpathian) origin, can be found in the Cretaceous successions of the Moldavide flysch of the Eastern Carpathians. These clasts, with the age of ca. 600 Ma, are attributed to a presumed ridge located in the flysch basin in the Early to Late Cretaceous period, to the Cuman Cordillera. Here, we present for the first time mineral chemistry data on these exotic igneous clasts, using the information in the present paper to discuss the geotectonic setting and P-T conditions during the formation of the igneous rocks that made up the basement of the disappeared paleorelief known as Cuman Cordillera. Selected samples of intrusive rocks were investigated by means of optical microscopy and electron microscopy. Biotite, feldspar and amphibole chemistry data were used for thermobarometry, indicating crystallization temperature at ca. 730-780°C and depth of magma emplacement around 10 km, within a possible range of 5-15 km. Biotite chemistry favors magma generation in convergent plate margins geotectonic setting.

Key words: Eastern Outer Carpathians, Moldavide nappes, Cuman Cordillera, exotic igneous clasts, thermobarometry

1. INTRODUCTION

The chemical composition of minerals has been used for a long time to estimate the physical conditions of metamorphism or magma generation and evolution. Biotite and amphibole compositions are among the most used data to get information for both temperature and pressure of magma crystallization (*e.g.*, Luhr *et al.*, 1984; Uchida *et al.*, 2007). Biotite can also be used to get insights into the geotectonic setting of magma crystallization (Abdel-Rahman, 1994; Shabani *et al.*, 2003) and, based on this, offering clues for the origin of detrital mineral grains containing biotite inclusions (*Bell et al.*, 2017).

Mineral chemistry is especially useful in the case of our study dedicated to certain disappeared forms of paleorelief, known as the Cuman Cordillera, whose existence was deduced only from the fragments of igneous rocks deposited in the sedimentary successions that cover the original continental crust. As the small size of these fragments commonly makes them not suitable for bulk rock chemistry investigations, the composition of minerals represents the most at hand source of information. Here, we provide mineral chemistry data (biotite, feldspar, amphibole) on rock fragments attributed to the Cuman Cordillera (Eastern Carpathians) and discussed on the possible significance of this information.

2. GEOLOGICAL SETTING AND PREVIOUS RESEARCH

The Moldavide nappes are situated in the external part of the Eastern Carpathians, being units with major tectogenesis in the Miocene. Their deformations began in the Late Cretaceous, being activated successively, therefore the deformation becomes younger eastwards. From the west to the east the nappes are the following: Teleajen (Convolute flysch), Macla, Audia, Tarcău, Vrancea (Marginal Folds), and

Subcarpathian. These nappes were made up of successions deposited over the thinned crust of the European passive continental margin. They are composed of sedimentary formations, mainly of flysch type and subordinately molasses, detached from their primary basement, and thrust outwards, over the units of the Carpathian Foreland (Săndulescu, 1984; Bădescu, 2005; Mațenco, 2017).

The igneous clasts from the Cretaceous successions of the Moldavide nappes that occur in the Eastern Carpathians were remarked during the interwar period as special occurrences, being described as red granites and porphyries. Murgeanu (1937) published a synthesis of the knowledge on their occurrence areas in the southern part of the Eastern Carpathians, between the valleys of Dâmbovița and Buzău rivers. He discussed the origins of red granites and porphyries and their accumulation in the sedimentary successions. The above-mentioned author argued for the exotic origin of these rocks, assuming that they were sourced from the Carpathian Foreland. He ascribed these igneous rocks to a ridge within the basin where the outer Eastern Carpathian flysch accumulated, which the author named the Cuman Cordillera. Filipescu and Alexandrescu (1962), supporting the exotic origin of the igneous clasts and the Cuman Cordillera model, documented the extent of the occurrence areas of the same types of igneous rock clasts as far to the north as Moldova Valley (northern part of Romania). The known occurrences of the rock fragments attributed to the Cuman Cordillera are given in figure 1. To note that previous studies on Zircon U-Pb geochronology indicated ages of ca. 600 Ma (Roban *et al.*, 2020; Lőrincz *et al.*, 2022).

For this study, we used samples from the Upper Cretaceous outcrops from Gurga Hill in the southern part of the Breaza locality (Fig. 2), previously investigated by Murgeanu (1937) and Codarcea (1937), therefore we were aware that the outcrops contained rocks with biotite and amphibole. The cropping out area of Upper Cretaceous rocks is surrounded by Paleogene formations (Murgeanu *et al.*, 1968), thus we presume that this region was uplifted by tectonic movements.

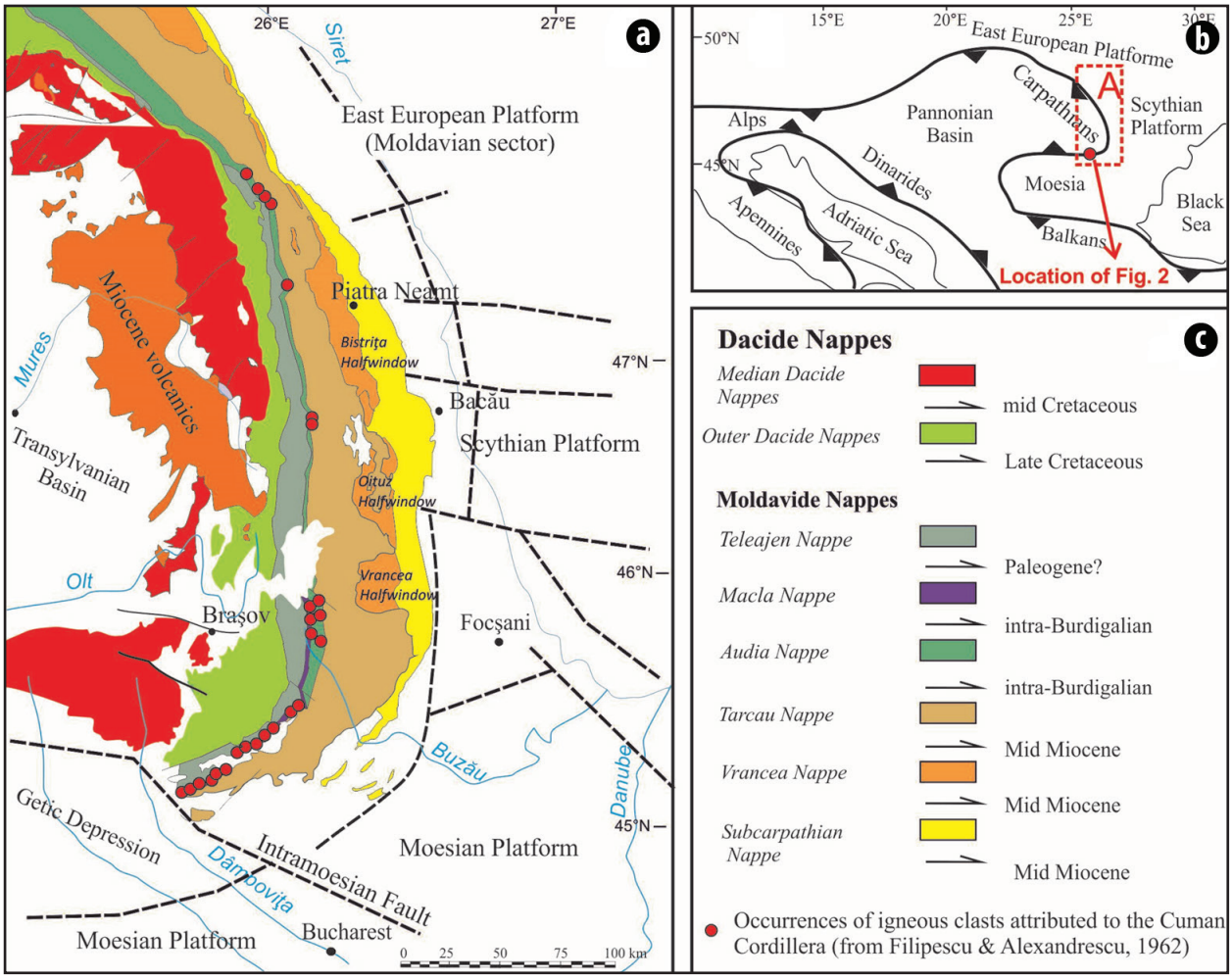

Fig. 1. (**a**) Known occurrences of the igneous clasts attributed to the Cuman ridge (Murgeanu, 1937; Filipescu and Alexandescu, 1962; data from our research). (**b**) Location of (a) within the Alpine orogenic belts of Europe. (**c**) Legend for A, with the indication of thrust age for each nappe. Tectonic map after Săndulescu, 1984; Bădescu, 2005; Mațenco, 2017.

In the Moldavides, a particular setting occurs in the southern part of the Eastern Carpathians, where the Macla Nappe is thrusted over a tectonic unit described as the Variegated Clay Nappe (Ştefănescu, 1995). This unit is interposed between Macla Nappe towards W and Tarcău Nappe at the E. The Variegated Clay Nappe is mainly composed of grey, red, and green clays, greenish marls, and calcareous sandstones. Granite, granodiorite, and felsic porphyry fragments occur as arkose, lens-like feldspar sands and gravels with fragments of felsic igneous rocks up to 10 cm in size. The largest fragments of igneous rocks are associated with a sandy limestone bed intercalated in the Variegated Clay Formation (Ştefănescu, 1995), being both intrusive (equigranular) and subvolcanic (porphyritic).

3. MATERIALS AND METHODS

The investigated outcrops are exposed in the Gurga Hill, south Breaza locality (Fig. 2), being mainly composed of red and white clays, containing also cm up to dm-thick limestones, towards the base (Fig. 3). The succession is rich in fragments of intrusive and porphyritic rocks. The age of sedimentary successions is argued based on the calcareous nannofossil content. Rich and well preserved nannofossil taxa indicate a Late Cretaceous age, Cenomanian towards the base and uppermost Cretaceous (Campanian to late Maastrichtian) to the upper part.

We investigated 25 fragments of both intrusive and porphyritic rocks. Thin and polished sections have been made from the collected samples of igneous rocks (both intrusive and porphyritic). These have been studied first using a Zeiss STEMI 508 stereo microscope and a Zeiss AXIO Imager A2m petrographic microscope, both provided with digital cameras connected to a desktop computer. We found not altered biotite crystals in 2 samples of intrusive rocks and amphibole that escaped alteration in only one sample of intrusive rocks.

The samples less affected by the alteration of component minerals were selected to be analyzed with a Zeiss Merlin Gemini II column Field Emission Scanning Electron Microscope (FE-SEM) equipped with an Oxford X-max50 EDS detector. The operating conditions were: an accelerating voltage of 20 kV, and a beam current of 2 nA.

4. RESULTS

The measured composition of the biotite and amphibole is shown in Tables 1-2. The mineral relations revealed a cumulate texture (Lőrincz *et al.*, 2022), with the potassium feldspar and quartz as intercumulus phases, and plagioclase, albite, biotite, apatite, and amphibole as cumulus phases (Figs. 4a to 4f).

In some samples, quartz has features of cumulus mineral relative to the potassium feldspar (Fig. 4e). Most mafic minerals are completely replaced by secondary minerals, whose assemblages provide information on their initial chemistry.

The amphiboles are replaced by chlorite, calcite (with some Mn and Fe), epidote, zoisite and sphene, preserving their euhedral shapes and the characteristic configuration of their cleavages (marked by chlorite stripes, Fig. 4b). The alteration assemblage suggests the initial calcic composition of the amphiboles, which is consistent with the composition of the few preserved amphibole crystals (Table 2) that is placed in a compositional field defined by edenite, ferroedenite, magnesiohornblende and ferrohornblende.

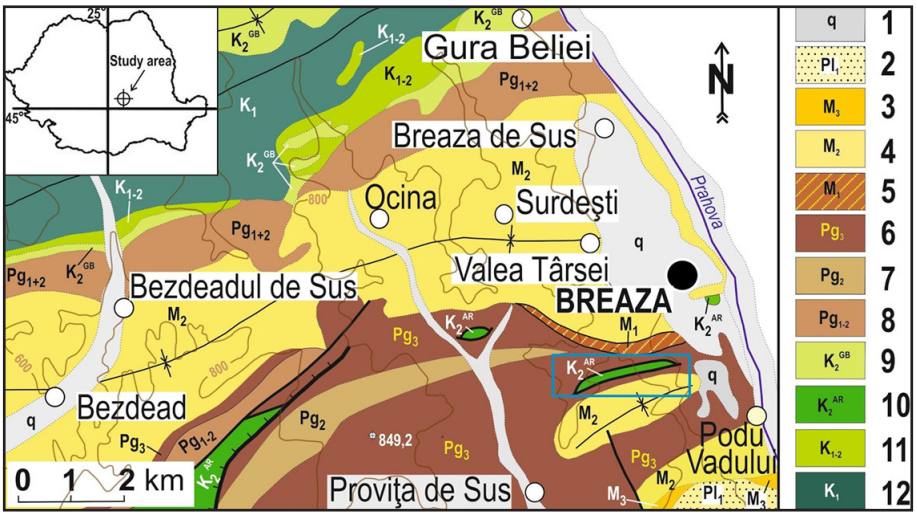

Fig. 2. Location of the cropping out area of the sampled formations south of Breaza (blue rectangle). Map after Murgeanu *et al.* (1968), with modifications. *Legend*: **1** – Quaternary; **2** – Lower Pliocene; **3** – Upper Miocene; **4** – Middle Miocene; **5** – Lower Miocene; **6** – Upper Paleogene; **7** – Middle Paleogene; **8** – Lower to Middle Paleogene; **9** – Uppermost Cretaceous, Gura Beliei Formation; **10** – Upper Cretaceous, Variegated Clay Formation; **11** – Lower to Upper Cretaceous (Outer Dacides); **12** – Lower Cretaceous. **1** to **10**: deposits of the post-tectonic cover of the Moldavide nappes; **11**-**12**: deposits of the Outer Dacide nappes.

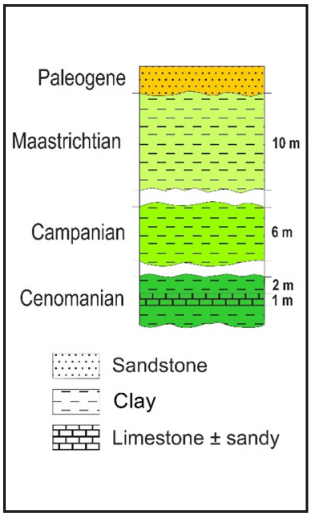

Fig. 3. Lithostratigraphy of the sampled outcrops at Breaza (composite). The age is based on calcareous nannofossil biostratigraphy.

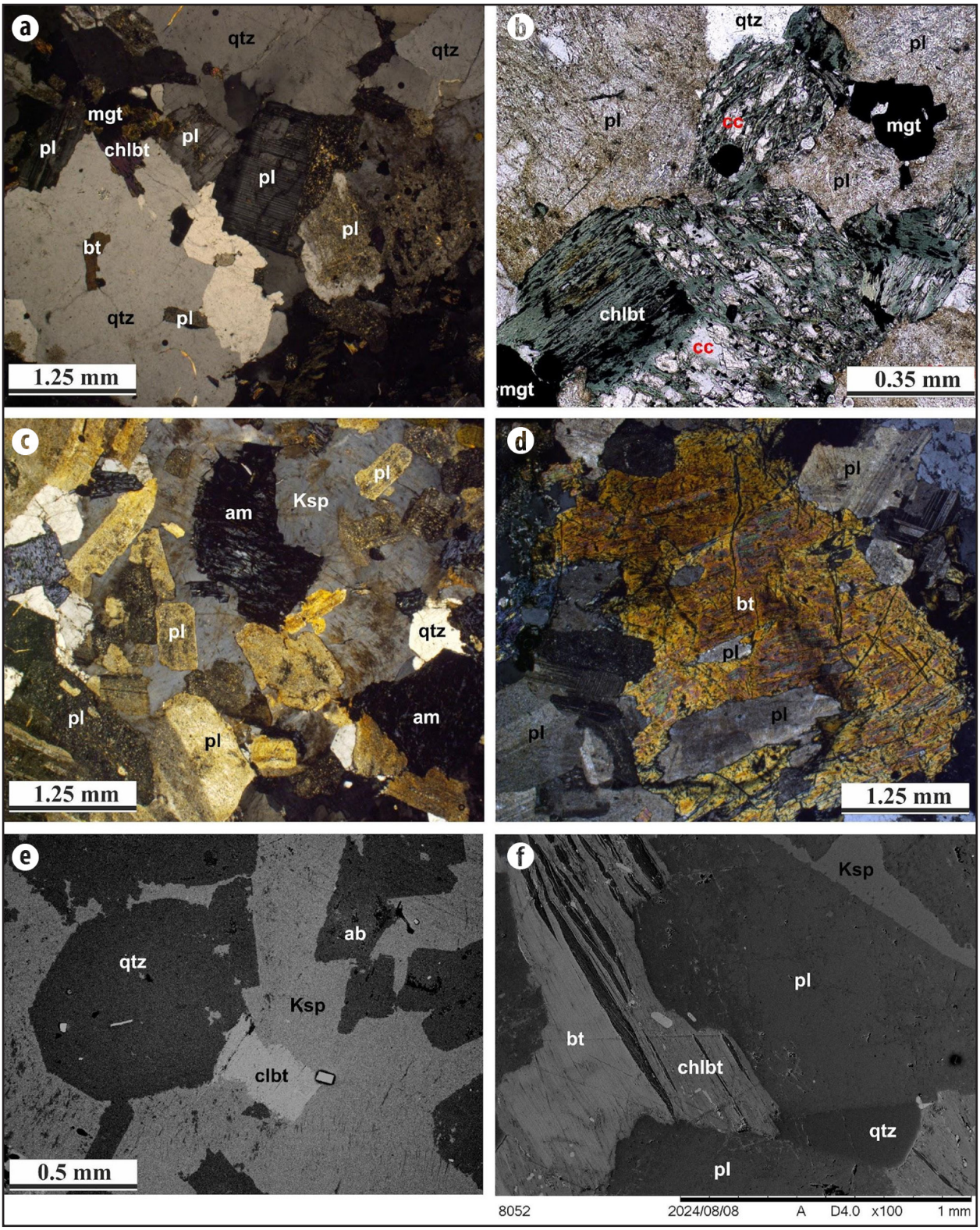

Fig. 4. Mineral relations. (**a**) Cumulus plagioclase and biotite in intercumulus quartz. (**b**) Intergrowth of amphibole (completely altered to chlorite and calcite), plagioclase and biotite (chloritized, with small unaltered relics). (**c**) Cumulus amphibole (completely altered) and plagioclase in intercumulus potassium feldspar. (**d**) Biotite with plagioclase inclusions. (**e**) Cumulus albite, biotite and euhedral quartz in intercumulus potassium feldspar. (**f**) Biotite with apatite inclusions partly engulfing plagioclase. *Abbreviations*: **ab** = albite; **bt** = biotite; **cc** = calcite; **chlbt** = chloritized biotite; **Ksp** = potassium feldspar; **mgt** = magnetite; **pl** = plagioclase; **qtz** = quartz.

Table 1. Biotite composition. The values for atoms per formula unit were calculated according to Li *et al.* (2020). Temperature based on Luhr *et al.* (1984), pressure based on Uchida *et al.* (2007).

Sample	51Z-21-46	51Z-22-11	51Z-32-26	51U-38-39	51U-38-59	51Z-50-58	51Z-52-20	51Z-53-39	51Z-53-52	51Z-54-00
SiO_2	36.92	36.96	36.37	36.67	36.78	35.29	35.39	35.74	35.53	35.96
TiO_2	4.92	5.06	5.19	4.25	3.84	4.46	3.84	4.01	3.90	3.97
Al_2O_3	13.29	13.36	13.55	15.22	15.4	13.30	14.00	14.02	13.75	13.87
FeO^T	23.48	23.40	24.94	20.84	21.81	23.95	23.49	23.28	22.93	22.69
MnO	0	0	0	0	0	0.80	0.58	0.58	0.78	0.62
MgO	8.62	8.58	7.33	10.89	11.31	8.15	9.76	9.52	8.99	9.23
K_2O	10.16	10.02	9.84	8.82	8.42	9.90	8.80	8.87	9.55	9.74
Fe_2O_{3calc}	4.05	4.05	4.31	4.48	5.71	5.33	7.42	7.18	7.44	6.32
FeO_{calc}	19.83	19.76	21.06	16.81	16.68	19.15	16.81	16.81	16.24	17.00
H_2O_{calc}	2.85	2.82	2.79	2.99	3.10	2.78	2.94	2.89	2.87	2.91
$Total_{calc}$	100.64	100.61	100.44	100.13	101.24	99.18	99.60	99.70	99.21	99.75
Based on 22 oxygen atoms										
T. Si	5.74	5.74	5.70	5.58	5.54	5.61	5.53	5.58	5.63	5.64
T.Al	1.81	1.83	1.85	2.14	2.15	1.98	1.96	1.92	1.75	1.82
$T.Fe^{3+}$	0.45	0.43	0.45	0.28	0.32	0.41	0.50	0.50	0.63	0.54
sum Tet	8	8	8	8	8	8	8	8	8	8
M.Al	0.62	0.62	0.65	0.59	0.58	0.51	0.62	0.66	0.82	0.74
M.Mg	2.03	2.02	1.77	2.45	2.49	2.03	2.36	2.31	2.34	2.31
$M.Fe^{2+}$	2.58	2.57	2.76	2.14	2.10	2.55	2.20	2.19	2.15	2.23
$M.Fe^{3+}$	0.03	0.04	0.06	0.23	0.33	0.23	0.37	0.34	0.26	0.21
M.Ti	0.56	0.57	0.59	0.47	0.42	0.51	0.43	0.45	0.45	0.45
M.Mn	0	0	0	0	0	0.11	0.08	0.08	0.10	0.08
sum oct	5.82	5.82	5.83	5.89	5.92	5.93	6.06	6.04	6.12	6.02
OH*	4.00	4.00	4.00	4.00	4.00	4.00	3.98	3.98	3.95	3.96
Fe^{3+}/Fe^T	0.31	0.31	0.31	0.39	0.47	0.40	0.57	0.56	0.58	0.50
Al total	2.43	2.45	2.50	2.73	2.73	2.49	2.58	2.58	2.57	2.56
Fe total	3.05	3.04	3.27	2.65	2.75	3.18	3.07	3.04	3.04	2.98
Fe/Fe+Mg	0.60	0.60	0.65	0.52	0.52	0.61	0.57	0.57	0.56	0.56
T (K)	1024.9	1033.6	1021.5	1031.2	1005.0	1006.4	1001.0	1012.3	1013.6	1007.9
(T°C)	752	760	748	758	732	733	728	739	740	735
P(kbar)	1.6	1.6	1.8	2.6	2.6	1.8	2.1	2.1	2.0	2.0

Table 2. Amphibole composition. Pressure calculation: P1 after Hammarstrom and Zen (1986); P2 after Mutch *et al.* (2016). Amphibole names follow Leake *et al.* (1997).

Sample	CC51Z-43	CC51Z-51	CC51Z-02	CC51Z-09	CC51Z-14	CC51-27	CC51Z-40	CC51-46	CC51Z-52	CC51Z-57	CC51Z-51a	CC51Z-17
SiO_2	42.46	42.71	43.05	42.33	42.82	44.22	43.66	44.21	43.16	43.67	42.93	44.18
TiO_2	1.54	1.60	1.53	1.65	1.54	1.35	1.56	1.46	1.72	1.74	1.73	1.36
Al_2O_3	8.50	8.30	8.02	8.40	8.19	8.03	8.69	8.31	8.47	9.24	9.13	8.29
FeO^T	20.09	20.06	19.87	20.57	20.26	19.68	19.97	19.87	19.73	20.14	21.14	20.01
MnO	1.02	0.93	0.95	0.96	0.92	1.00	0.96	0.98	0.87	0.86	0.99	0.90
MgO	8.57	8.75	8.73	8.26	8.49	9.46	8.99	9.45	8.84	9.09	8.38	9.18
CaO	11.21	11.31	11.47	11.35	11.57	11.54	11.45	11.56	11.30	11.18	11.45	11.47
Na_2O	1.43	1.27	1.22	1.16	1.23	1.31	1.43	1.39	1.26	1.49	1.48	1.26
K_2O	1.04	0.90	0.95	0.99	0.94	0.92	0.98	0.89	0.91	0.90	1.00	0.91
Cl	0.17	0.13	0.13	0.18	0.14	0.14	0.18	0.12	0.11	0.13	0.15	0.13
Total	96.01	95.96	95.92	95.85	96.09	97.64	97.86	98.23	96.37	98.46	98.38	97.69
Based on 23 oxygen atoms												
Si	6.597	6.616	6.677	6.592	6.644	6.706	6.633	6.665	6.645	6.571	6.521	6.699
AlIV	1.403	1.384	1.323	1.408	1.356	1.294	1.367	1.335	1.355	1.429	1.479	1.301
Sum T	8.000	8.000	8.000	8.000	8.000	8.000	8.000	8.000	8.000	8.000	8.000	8.000
Al VI	0.153	0.131	0.143	0.133	0.142	0.141	0.188	0.142	0.181	0.210	0.155	0.181
Ti	0.179	0.186	0.179	0.193	0.180	0.154	0.178	0.166	0.199	0.197	0.198	0.155
Fe^{3+}	0.398	0.452	0.368	0.456	0.381	0.416	0.358	0.425	0.367	0.426	0.444	0.408
Mg	1.985	2.020	2.020	1.919	1.964	2.138	2.036	2.124	2.029	2.040	1.898	2.075
Fe^{2+}	2.212	2.146	2.210	2.224	2.249	2.081	2.180	2.080	2.173	2.109	2.241	2.130
Mn	0.072	0.064	0.081	0.077	0.084	0.070	0.060	0.064	0.050	0.018	0.064	0.052
Sum C	5.000	5.000	5.000	5.000	5.000	5.000	5.000	5.000	5.000	5.000	5.000	5.000
Mn	0.062	0.057	0.043	0.050	0.036	0.058	0.063	0.061	0.064	0.092	0.064	0.064
Ca	1.866	1.877	1.907	1.894	1.923	1.875	1.865	1.869	1.864	1.803	1.864	1.864
Na	0.071	0.066	0.050	0.057	0.041	0.067	0.072	0.070	0.073	0.105	0.073	0.073
SumB	2.000	2.000	2.000	2.000	2.000	2.000	2.000	2.000	2.000	2.000	2.000	2.000
Na	0.359	0.315	0.316	0.294	0.329	0.318	0.348	0.336	0.303	0.330	0.363	0.299
K	0.205	0.178	0.188	0.197	0.186	0.177	0.190	0.171	0.179	0.173	0.194	0.176
SumA	0.564	0.494	0.505	0.491	0.515	0.495	0.537	0.508	0.482	0.503	0.556	0.475
Total	15.564	15.494	15.505	15.491	15.515	15.495	15.537	15.508	15.482	15.503	15.556	15.475
Cl	0.044	0.036	0.034	0.048	0.037	0.037	0.046	0.031	0.028	0.034	0.040	0.034
OH	2.044	2.036	2.034	2.048	2.037	2.037	2.046	2.031	2.028	2.034	2.040	2.034
Total	17.653	17.565	17.572	17.588	17.588	17.570	17.629	17.569	17.537	17.570	17.636	17.542
Name	Ferro-edenite	Ferrohbd	Ferro-edenite	Ferrohbd	Ferro-edenite	Mg-hbd	Ferro-edenite	Edenite	Ferrohbd	Ferro-edenite	Ferro-edenite	Ferrohbd
AlT	1.556	1.515	1.465	1.541	1.498	1.435	1.556	1.477	1.536	1.639	1.634	1.481
P1 kb (H+Z)	3.9	3.7	3.5	3.8	3.6	3.3	3.9	3.5	3.8	4.3	4.3	3.5
P2 kb	3.4	3.3	3.1	3.4	3.2	3.0	3.4	3.2	3.4	3.7	3.7	3.2

Biotite is often transformed into chlorite, preserving the primary inclusions of apatite and zircon. Nevertheless, biotite is generally better preserved compared with the amphibole. Its composition (Table 1) is characterized by high Ti and Fe contents (3.84-5.19% TiO_2 and 20.84-24.94% FeO^T).

The composition of feldspars from the samples that contain the biotite and amphibole reported in this work is illustrated in figure 5. In these samples, the plagioclase shows the most anorthite-rich compositions in all the 25 investigated samples, dominated by andesine, but also with some labradorite compositions.

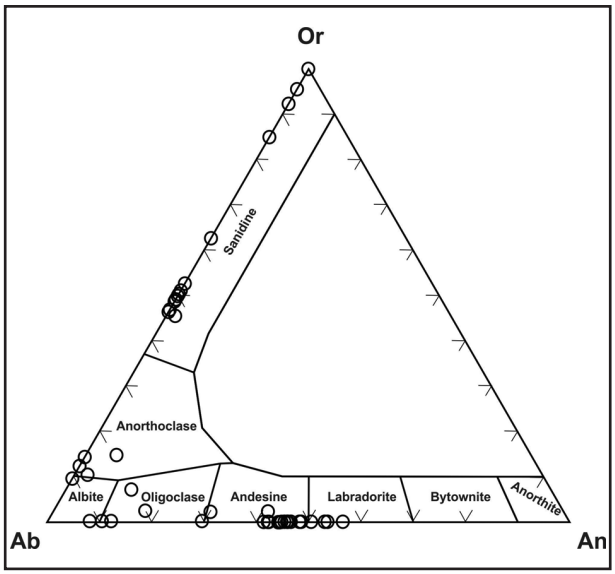

Fig. 5. Feldspar composition in the rocks that contained the biotite and amphibole whose composition is reported in this research.

5. DISCUSSION

The cumulate texture of the intrusive rocks gives information regarding the order of crystallization. The potassium feldspar was the last to crystallize, preceded by quartz. The plagioclase was among the first to crystallize, possibly at the same time as the amphibole, which suggests that the two minerals could have been in equilibrium during their crystallization. There are spatial relations indicating biotite crystallization after plagioclase (Figs. 4d, 4f). Apatite occurs as inclusions in almost all other minerals, except for plagioclase.

5.1. Thermobarometry

We used the mineral chemistry data to reveal information regarding the crystallization conditions and type of geotectonic setting. Biotite is one mineral that can provide such information, especially for granitoid rocks, if it was not re-equilibrated after the magmatic stage. Several studies (*e.g.*, Perchuk and Lavrent'eva, 1983; Hoisch, 1989; Holdaway, 2000; Wu and Cheng, 2006; Samadi *et al.*, 2021) showed that biotite composition can be altered by the chemical exchange with muscovite and/or garnet. The biotite we investigated occurs in rocks that do not contain muscovite or garnet; therefore, it is reasonable to consider that it preserved its original composition. The method based on Fe, Mn, Ti, and Mg contents, elaborated by Nachit *et al.* (2005) to verify the possibility of post-magmatic biotite re-equilibration was used by several authors (*e.g.*, Sarjoughian *et al.*, 2015; Bayati *et al.*, 2017; Dubosq *et al.*, 2019; Nalluri *et al.*, 2022). In figure 6, the biotite from the analyzed igneous rocks, attributed to the Cuman Cordillera, plots in the field of magmatic biotite.

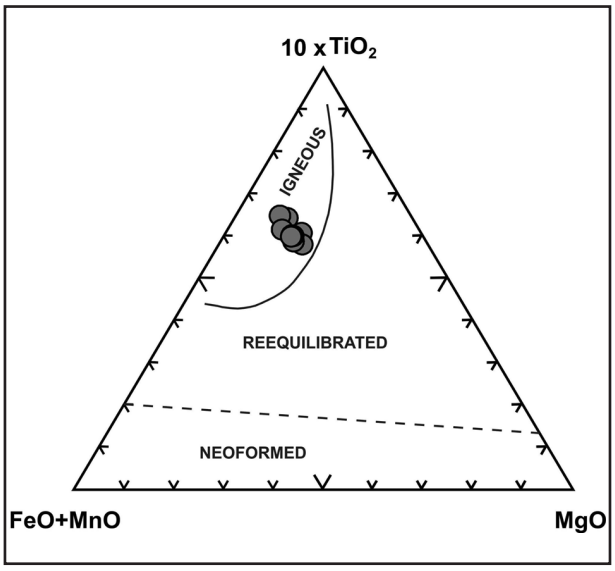

Fig. 6. Plot of the biotite composition on the diagram recommended by Nahit *et al.* (2005) to distinguish the igneous biotite from the reequilibrated and neoformed biotite.

Carmichael, in a study dedicated to El Chichon volcano (Luhr *et al.*, 1984), formulated the following geothermometer based on a coupled exchange of Fe and Ti in biotite (apfu based on 22 oxygen atoms):

$$T(°K) = 838/(1.0337 - Ti/Fe^{2+}) \quad (1)$$

Using this formula, we got temperatures between 728°C and 760°C (Table 1).

Biotite composition can provide information on the pressure during its crystallization. Uchida *et al.* (2007) showed that total Al content of biotite can be used to estimate the solidification pressure of the granitic rocks, proposing the following empirical formula:

$$P(kbar) = 3.33 \times {}^{T}Al - 6.53 (\pm 0.33) \quad (2)$$

where ^{T}Al is total aluminum (apfu based on 22 oxygen atoms). Using this formula, we obtained pressure values between 1.3 kbar and 2.9 kbar (Table 1), i.e., depths of 5-10 km.

Aluminum content in hornblende is used to estimate the pressure during crystallization in granites containing the mineral assemblage: amphibole + plagioclase (An_{15-80}) + biotite + quartz + alkali feldspar + ilmenite/sphene + magnetite + apatite. The granitoids we investigated contain this mineral assemblage. Hammarstrom and Zen (1986)

proposed the following formula for pressure estimation based on Al content in hornblende:

$$P(kbar) = -3.92 + 5.03 \times Al^T \quad (3)$$

where Al^T represents the total Al atoms per formula unit (per 23 oxygens). Based on this formula, pressure values of 3.3 kbar to 4.3 kbar have been determined (P1 in Table 2), i.e. depths of 10-15 km.

Mutsch *et al.* (2016) refined the estimation of pressure calculation based on Al in hornblende, recommending the formula:

$$P\ (kbar) = 0.5 + 0.331 \times Al^T + 0.995 \times (Al^T)^2 \quad (4)$$

This formula, applied to the amphiboles we investigated, produced pressure values of 3.0 kbar to 3.7 kbar (P2 in Table 2), i.e., crystallization depths exceeding 10 km. There is a difference between the pressure indicated by Al in biotite and the pressure determined by Al in hornblende, the former being lower than the latter. This might be explained by a series of factors involving the post-emplacement changes of the magmatic composition of the minerals but could also be related to the timing of the crystallization. As the mineral relations suggest biotite crystallization later than plagioclase, and amphibole crystallization contemporaneous with the plagioclase, there is a possibility that biotite recorded a stage of magma ascent to shallower depth in the crust.

The temperature estimations made on the hornblende-plagioclase thermometry (Blundy and Powell, 1990) indicated temperatures of 760-780°C for pressures of ca. 3 kbar, which is consistent with the temperature indicated by biotite composition.

5.2. Geotectonic considerations

Biotite composition can be used as indicator of the geotectonic setting of magma generation. Abdel-Rahman (1994), based on the fact that biotite composition depends on the nature of magma from which it crystallized and on a large number of measured biotite compositions from different types of granitic bodies, defined compositional fields in the FeO^T-MgO-Al_2O_3 ternary diagram, corresponding to A-type granites, calc-alkaline (I-type) granites and peraluminous (S-type) granites.

Subsequently, many authors (*e.g.*, Aydin *et al.*, 2003; Parsapoor *et al.*, 2015; Bayati *et al.*, 2017; Shellnutt *et al.*, 2020; Nalluri *et al.*, 2022) used this diagram to discriminate between the geotectonic settings of magma emplacement.. In figure 7, the investigated biotite from the clasts attributed to the Cuman Cordillera plots in the field of calc-alkaline granites (I-type), also suggesting more affinities with the A-type granites than with the peraluminous granites generated by the melting of sedimentary rocks.

Shabani *et al.* (2003) used the annite-siderophyllite-phlogopite-eastonite quadrilateral to plot the atoms per formula unit values of total Al versus $Fe^{2+}/(Fe^{2+}+Mg)$ for biotite from different granitic rocks and defined fields characteristic for A-type (within plate), continental arc, and strongly contaminated and reduced I type granitic suites. The biotite from our samples plots within the continental arc field, mostly in zones of overlapping with either within-plate (A-type) granites (most compositions) or strongly contaminated and reduced I-type granites (Fig. 8). These features agree with the I-type mineral assemblage of the investigated granites (Lőrincz *et al.*, 2022), including amphibole, biotite and sphene, but no muscovite.

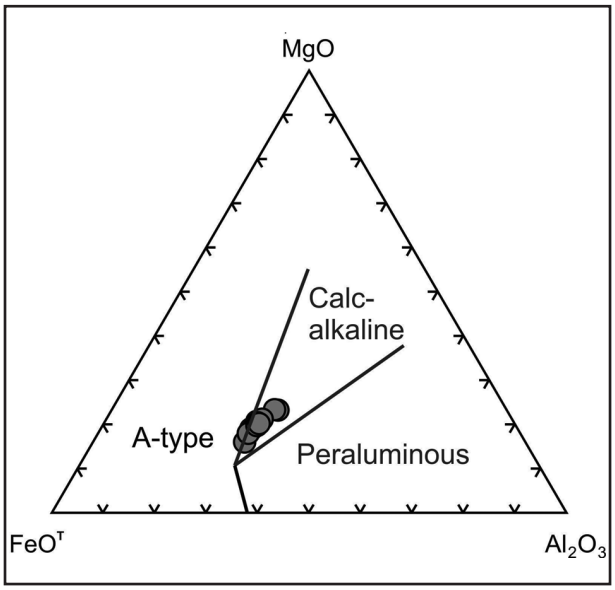

Fig. 7. Ternary plot of biotite composition. The separation of the compositional fields of A-type granites, calc-alkaline granites and peraluminous granites after Abdel-Rahman (1994). $FeO^T = FeO + Fe_2O_3$ x 0.89981.

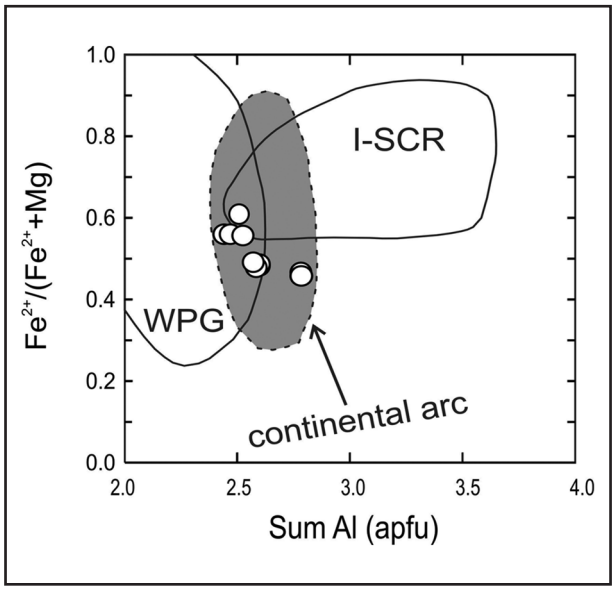

Fig. 8. Plot of biotite compositional features. The compositional fields of within-plate granites (A-type), continental arc granites and I-SCR (strongly contaminated and reduced I-type) granites after Shabani *et al.* (2003).

6. CONCLUSIONS

The first mineral chemistry data on the clasts of magmatic origin attributed to the Cuman Ridge, reported here, allowed some deductions on the conditions and geological setting of magma evolution. Magma temperature, determined from biotite composition and from the use of hornblende-plagioclase thermometry, is 730-780°C. The depth of emplacement is around 10 km; it could have been shallower than 10 km (as indicated by the Al in biotite method) or deeper than 10 km (as suggested by the Al in hornblende geobarometry), but within a total range of 5-15 km.

Biotite chemistry favors magma generation in association with a geodynamic setting of convergent plate margins. The results of these study provide reasons to extend the research on mineral chemistry to other occurrences of igneous clasts attributed to the Cuman Cordillera.

ACKNOWLEDGEMENTS

The authors are grateful to Dr. Mihaela Melinte-Dobrinescu, who made the calcareous nannofossil biostratigraphy and to Dr. Valentina Cetean, for all the support given in carrying out our research.

REFERENCES

Abdel-Rahman, A.-F.M. (1994). Nature of biotites from alkaline, calc-alkaline, and peraluminous magmas. *Journal of Petrology*, **35**: 525-541.

Bădescu, D. (2005). Evoluția tectono-stratigrafică a Carpaților Orientali în decursul Mezozoicului și Neozoicului. Editura Economică, 312 p.

Bell, E.A., Boehnke, P., Harrison T.M. (2017). Applications of biotite inclusion composition to zircon provenance determination. *Earth and Planetary Science Letters*, **473**: 237-246.

Blundy, J.D., Holland, T.J.B. (1990). Calcic amphibole equilibria and a new amphibole-plagioclase geothermometer. *Contributions to Mineralogy and Petrology*, **104**: 208-224.

Codarcea, A. (1937). Étude micrographique des roches cristallines du Sénonien de Breaza. *Comptes rendus des séances de l'Institut Géologique de Roumanie*, Tome XXI, 85 p.

Filipescu, M.G., Alexandrescu, G. (1962). Distribution of the coarse sandstones and arkoses with red feldspar in the Cretaceous of the Eastern Carpathians (in Romanian). *Studii și cercetări de geologie, geofizică, geografie, Series Geologie*, **7**(*2*): 241-248.

Hoisch, T.D. (1989). A muscovite-biotite geothermometer. *American Mineralogist*, **74**: 565-572.

Holdaway, M.J. (2000). Application of new experimental and garnet Margules data to the garnet-biotite geothermometer. *American Mineralogist* **85**: 881-892.

Le Maître (Ed.) (1989). A classification of igneous rocks and glossary of terms. *Blackwell Scientific Publications, Oxford*, 193 p.

Leake, B.E., Wooley, A.R., Arps, C.E.S., Birch, W.D., Gilbert, M.C., Grice, M.C., Hawthorne, F.C., Kato, A., Kisch, H.J., Krivovichev, V.G., Linthout, K., Laird, J., Mandarino, J., Maresch, W.V., Nickel, E.H., Rock, N.M.S., Schumacher, J.C., Smith, D.C., Stephenson, N.C.N., Ungaretti, L., Whittaker, E.J.W., Youzhi, G. (1997). Nomenclature of the Amphiboles. Report of the Subcommittee on Amphiboles of the International Mineralogical Association Commission on New Minerals and Mineral Names. *European Journal of Mineralogy*, **9**: 623-651.

Li, X., Zhang, C., Behrens, H., Holtz, F. (2020). Calculating biotite formula from electron microprobe analysis data using a machine learning method based on principal components regression. *Lithos*, **356-357**: 105371.

Lőrincz, S., Melinte-Dobrinescu, M., Roban, R-D., Ducea, M., Cetean, V., Munteanu, M., Ene, V-V. (2022). Magmatic clasts from turbidites in the Moldavide nappes as indication of a late Proterozoic subduction event in the foreland of the Eastern Carpathians. Goldschmidt Conference 2022, Honolulu, Hawaii, htttp://doi.org./10.46427/gold2022.10869

Luhr, J. F., Carmichael, I.S.E., Varekamp, J. C. (1984). The 1982 eruptions of El Chichón volcano, Chiapas, Mexico: mineralogy and petrology of the anhydrite-bearing pumices. *Journal of Volcanology and Geothermal Research*, **23**: 69-108.

Matenco, L. (2017). Tectonics and exhumation of Romanian Carpathians: Inferences from kinematic and thermochronological studies. In M. Rădoane and A. Vespremeanu-Stroe (Eds.), *Landform dynamics and evolution in Romania*: 15-56, Springer International Publishing.

Murgeanu, G. (1937). Sur une cordilière ante-sénonienne dans le geosynclinal du flysch carpatique. *Dări de seamă ale ședințelor Institutului Geologic al României*, **XXI**: 69-85.

Murgeanu, G., Patrulius, D., Gherasi, N., Ghenea, C., Ghenea, A. (1968). Geological Map of Romania, scale 1:200,000, Târgoviște Sheet, Geological Institute of Romania.

Mutch, E.J.F., Blundy, J.D., Tattitch, B.C., Cooper, F.J., Brooker, R.A. (2016). An experimental study of amphibole stability in low-pressure granitic magmas and a revised Al-in-hornblende geobarometer. *Contributions to Mineralogy and Petrology*, **171**: 85.

Nachit, H., Ibhi, A., Abia, E.H., Ohoud, M.B. (2005). Discrimination between primary magmatic biotites, reequilibrated biotites and neoformed biotites. *Comptes Rendues Geoscience*, **337**: 1415-1420.

Perchuk, L., Lavrent'eva, V. (1983). Experimental investigation of exchange equilibria in the system cordierite-garnet-biotite. *In*:

Saxena, S.K. (Ed.), Kinetics and Equilibrium in Mineral Reactions. *Advances in Physical Geochemistry*, **3**: 199-239.

Roban, R.D., Ducea, M.N., Mațenco, L., Panaiotu, G.C., Profeta, L., Krézsek, C., Melinte-Dobrinescu, M.C., Anastasiu, N., Dimofte, D., Apotrosoaiei, V., Francovschi, I. (2020). Lower Cretaceous provenance and sedimentary deposition in the Eastern Carpathians: Inferences for the evolution of the subducted oceanic domain and its European passive continental margin. *Tectonics*, **39**: e2019TC005780.

Samadi, R., Torabi, G., Kawabata, H., Miller, N.R. (2021). Biotite as a petrogenetic discriminator. Chemical insights from igneous, meta-igneous and meta-sedimentary rocks in Iran. *Lithos*, **386-387**: 106016.

Săndulescu, M. (1984). Geotectonica României. Editura Tehnică București, 336 p.

Shabani, A.A.T., Lalonde, A., Whalen, J.B. (2003). Composition of biotite from granitic rocks of the Canadian Appalachian Orogen: a potential tectonomagmatic indicator. *Canadian Mineralogist*, **41**: 1381-1396.

Shellnutt, J.G., Vaughan, M.W., Lee. H-Y., Iizuka, Y. (2020). Late Jurassic leucogranites of Macau (SE China): A record of crustal recycling during the Early Yanshanian orogeny. *Frontiers in Earth Science*, **8**: 311.

Ștefănescu, M. (1995). Stratigraphy and structure of Cretaceous and Paleogene flysch deposits between Prahova and Ialomița valleys. *Romanian Journal of Tectonics and Regional Geology*, **76**: 4-49.

Uchida, E., Endo, S., Makino, M. (2007). Relationship between solidification depth of granitic rocks and formation of hydrothermal ore deposits. *Resource Geology*, **57**: 47-56.

Wu, C.M., Cheng, B.H. (2006). Valid garnet-biotite (GB) geothermometry and garnetaluminum silicate-plagioclase-quartz (GASP) geobarometry in metapelitic rocks. *Lithos*, **89**: 1-23.